Whistler Waves at Venus's Quasi-Parallel Bow Shock

B. Page[1,2], T.A. Bowen[2], S.D. Bale[1,2,3,4], J.W. Bonnell[2], A. Case[5], T. Dudok de Wit[6], K. Goetz[7], K. Goodrich[2], J. Halekas[8], P.R. Harvey[2], J.C. Kasper[9], D. Larson[2], R.J. MacDowall[10], D.M. Malaspina[11,12], M. Oka[2], M. Pulupa[2], P. Whittlesey[2]

[1]Physics Department, University of California, Berkeley, CA 94720-7300, USA
[2]Space Sciences Laboratory, University of California, Berkeley, CA 94720-7450, USA
[3]The Blackett Laboratory, Imperial College London, London, SW7 2AZ, UK
[4]School of Physics and Astronomy, Queen Mary University of London, London E1 4NS, UK
[5]Smithsonian Astrophysical Observatory, Cambridge, MA 02138 USA
[6]LPC2E, CNRS and University of Orléans, Orleans, France
[7]School of Physics and Astronomy, University of Minnesota, Minneapolis, MN 55455, USA
[8]Department of Physics and Astronomy, University of Iowa, Iowa City, IA 52242, USA
[9]Climate and Space Sciences and Engineering, University of Michigan, Ann Arbor, MI 48109, USA
[10]Solar System Exploration Division, NASA/Goddard Space Flight Center, Greenbelt, MD, 20771
[11]Laboratory for Atmospheric and Space Physics, University of Colorado, Boulder, CO 80303, USA
[12]Astrophysical and Planetary Sciences Department, University of Colorado, Boulder, CO, USA

Key Points:

- Whistler wave growth patterns within the Venusian bow shock have some similarities with those in Earth's bow shock.
- Some whistler waves downstream of the Venusian bow shock propagate at angles more than 80° oblique to the background magnetic field.
- These waves have elliptical magnetic field polarization that is found to be in strong agreement with predictions from kinetic theory.

Corresponding author: Brent Page, `brent_page@berkeley.edu`

Abstract

In planetary bow shocks, binary particle collisions cannot mediate the conversion of upstream bulk flow energy into downstream thermal energy, and wave-particle interactions in part assume this role. Understanding the contribution of waves to shock heating requires knowledge of the modes that propagate in different classes of shocks; we describe the growth patterns of whistler waves within the Venusian bow shock. Waves with frequencies $f \lesssim 0.1 f_{ce}$, where f_{ce} is the electron cyclotron frequency, preferentially grow at local minima in the background magnetic field $|B_0|$. Quasi-parallel propagating whistlers with frequencies between $0.1 f_{ce}$ and $0.3 f_{ce}$ are strongest at the downstream ramps of these $|B_0|$ minima. Immediately downstream of the shock, whistlers with frequencies $f < 0.1 f_{ce}$ propagate more than 80° oblique from $\vec{B}_0$ and have elliptically polarized $\vec{B}$ fields. A prediction from kinetic theory of the orientation of these waves' $\vec{B}$ ellipses is confirmed to high accuracy.

Plain Language Summary

When particles moving faster than the speed of sound encounter an obstacle, a shock wave forms. This happens, for example, when the electrons and protons streaming away from the Sun flow into planets. When particles pass through a shock wave, their temperature increases and their flow speed decreases. This heating and slowing process is in part mediated by the interaction between collective particle motions (i.e. waves) and individual particles. One type of wave that propagates within and near astrophysical shocks, called a whistler wave, consists of electrons revolving in concert with rotating electric and magnetic fields. This wave is generated in many of the same locations at Venus's shock as at Earth's. Also, the wave's magnetic field rotates in an ellipse instead of a circle when the wave's propagation direction is sufficiently unaligned with the background magnetic field.

1 Introduction

The first examination of whistler waves at Venus was stimulated by measurements from *Pioneer Venus* of 100 Hz electric field power in the planet's magnetosheath (Scarf et al., 1980). These waves were initially suspected to be whistlers, but a lack of coinciding magnetic field measurements prevented definitive mode identification, and they have also been suspected to be lower hybrid waves (Szegö et al., 1991) and ion-acoustic waves (Strangeway & Crawford, 1993).

Venus Express observed 1 Hz circularly polarized magnetic field fluctuations upstream of the bow shock consistent with Doppler shifted whistlers (Orlowski & Russell, 1991; Xiao et al., 2020). These waves have many similarities with 1 Hz waves seen in the corresponding region at Earth, and are thought to grow at the shock and damp out as they propagate upstream.

We focus on whistler waves in the bow shock and compare our observations with those of Pioneer Venus and Venus Express when possible, but primarily use measurements of Earth's bow shock to provide context. Whistler waves have been documented more extensively at Earth than at Venus (e.g. Olson et al., 1969; Holzer et al., 1972; Rodriguez & Gurnett, 1975), and contemporary observatories at Earth such as the Magnetospheric Multiscale (MMS) mission provide a detailed view of wave-fields and particle dynamics (Burch et al., 2016).

Two bands of whistler waves are found in Earth's perpendicular bow shock: one propagating quasi-parallel to $\vec{B}_0$ with $f > 0.1 f_{ce}$ and another propagating oblique to $\vec{B}_0$ with $f \lesssim 0.1 f_{ce}$ (e.g. Y. Zhang et al., 1999; Hull et al., 2012, 2020; Wilson III et al., 2014). The low frequency whistlers are sufficiently strong ($\Delta B/|B_0| \sim 0.1 - 1$) to

affect the macroscopic magnetic structure of the shock, and their magnetic field minima are correlated with the higher frequency waves (Hull et al., 2012, 2020).

Simulations show that the large $|B|$ gradients of the $f \lesssim 0.1 f_{ce}$ waves scatter electrons, thereby trapping them in $|B|$ minima, where they have a perpendicular temperature anisotropy that may generate the high frequency whistlers (e.g. Oka et al., 2019). The high frequency waves, in turn, scatter electrons via cyclotron resonance (e.g. Oka et al., 2017).

Parker Solar Probe's (PSP's) measurements in the Venusian shock show a similarly structured spectrum of whistler waves, suggesting that the electron acceleration mechanisms operating at Earth may also operate here. Similarities in dynamics at Venus and Earth also point to universal processes in magnetized collisionless shocks, insensitive to such factors as the solar wind density, the upstream magnetic field strength, or the presence of a planetary magnetic field.

In addition, directly downstream of the shock discontinuity in $\vec{B}_0$, PSP's observations reveal whistlers with $f \lesssim 0.1 f_{ce}$ that propagate $\sim 80°$ oblique to $\vec{B}_0$ with magnetic field ellipticity < 0.6. The orientations of the semimajor and semiminor axes of these waves' $\vec{B}$ fields strongly agree with predictions from kinetic theory (Verkhoglyadova et al., 2013; Remya et al., 2016).

2 Data

Although it is primarily designed to study the Sun, PSP will also take measurements in the bow shock, magnetosheath, magnetosphere, and upper ionosphere of Venus over seven planned flybys. Each flyby, or Venus Gravity Assist (VGA), transfers some of PSP's orbital energy to the planet, decreasing PSP's distance to the Sun at perihelion. We use data from the first VGA, which is illustrated in Figure 1.a.

The FIELDS instrument on PSP measures the magnetic field from DC to 293 Hz using two fluxgate magnetometers and from 10 Hz to 50 kHz using a search-coil magnetometer (Bale et al., 2016). The SCaM data product, which is used for this study, merges the measurements from these two instruments to produce time series data that put high frequency oscillations into the context of the background field variations (Bowen et al., 2020).

FIELDS measures the electric field in two coordinate directions using four 2 m antennas. They are arranged into two approximately orthogonal dipoles, each consisting of two antennas mounted 3 m from one another. During the time period studied, the Digital Fields Board component of FIELDS continuously sampled these dipoles at 293 Hz (Malaspina et al., 2016).

Minimum Variance Analysis (MVA) of the magnetic field is used to determine wave propagation angles relative to the background magnetic field $\vec{B}_0$ (Sonnerup & Scheible, 1998). For an elliptically polarized wave, MVA finds the axis around which $\vec{B}$ is polarized, thereby determining $\hat{k}$ with a 180° ambiguity. MVA's results are quoted using the symbol $\theta_{\pm\vec{k}-\vec{B}_0}$, which denotes either the angle between $\vec{k}$ and $\vec{B}_0$ or the angle between $-\vec{k}$ and $\vec{B}_0$ – whichever is smaller.

The SWEAP instrument suite characterizes the electron and ion populations encountered by PSP (Kasper et al., 2016). A pair of electrostatic analyzers (SPAN-E) measure the full 3D electron velocity distribution function; we use SPAN-E's estimates of the electron density and temperature (Whittlesey et al., 2020). We also use measurements of the proton density, proton temperature, and bulk plasma velocity from the Faraday cup (SPC) component of SWEAP (Case et al., 2020).

3 Whistler Wave Activity at the Bow Shock

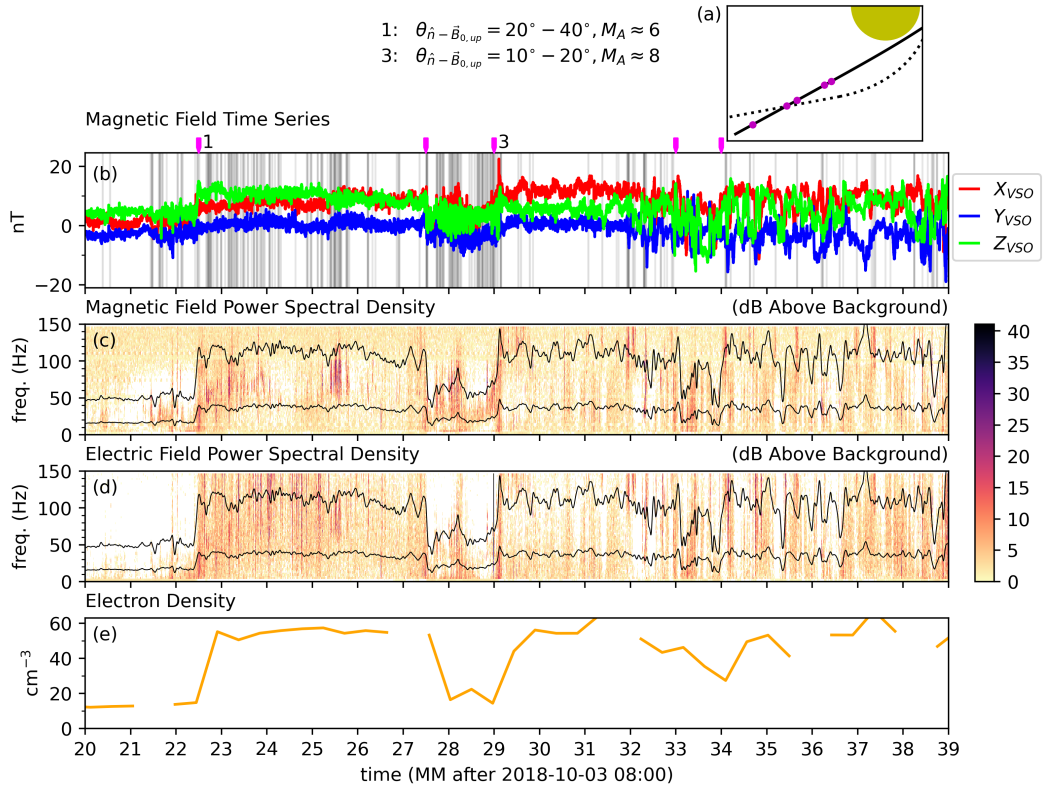

Figure 1. Panel (a): the flyby geometry. The solid black line is PSP's trajectory; it starts at the bottom left, which is anti-sunward and dawnward of Venus (yellow circle). The trajectory lies approximately in the ecliptic. A global bow shock model from T. Zhang et al. (2008) is shown with a dotted line. The bow shock locations from PSP's flyby are marked by purple dots, which correspond to the purple hashes above panel (b). We focus on the bow shock crossings labeled 1 and 3, whose shock normal angles and Alfvén Mach numbers are listed at the top of the Figure. The magnetic field in panel (b) is in VSO coordinates, and the gray shading marks locations of whistler waves. Panel (c): The power spectral density (PSD) of the magnetic field in dB above a background averaged over the surrounding three minutes of each spectrum. The black lines mark $0.1f_{ce}$ and $0.3f_{ce}$; they are Gaussian smoothed with a standard deviation of 1 s in order to avoid obscuring the spectra. Panel (d): The PSD of the electric field normalized in the same manner as the $\vec{B}$ PSD. This normalization diminishes continuous electrostatic power in the magnetosheath that extends from DC to the 150 Hz Nyquist frequency. These broadband emissions and the more narrowband electromagnetic power in panels (c) and (d) likely both contributed to the 100 Hz electric activity reported in (Scarf et al., 1980). Panel (e): the electron density moment. The time resolution is about one measurement every 28 seconds; data gaps are present in regions of high moment uncertainty.

Whistler emissions during PSP's flyby of Venus began roughly a minute prior to the first bow shock crossing, which corresponds to a displacement of 0.24 r_v in the anti-sunward direction and 0.13 r_v in the dawn direction, where r_v is the radius of Venus. At low frequencies, both $\vec{E}$ and $\vec{B}$ feature erratic fluctuations with spectral peaks near 1 Hz. The wave amplitude ΔB is 1-2 nT in a 6 nT background field, and MVA over single wave

cycles shows circular polarization of $\vec{B}$ with $\theta_{\pm\vec{k}-\vec{B}_0} \sim 30°$. 1 Hz whistlers have been detected before in the upstream regions of Venus (Orlowski & Russell, 1991; Xiao et al., 2020), Mars (Brain et al., 2002), and Earth (e.g. Fairfield, 1974), almost exclusively in areas magnetically connected to the shock. We observe them to be strongest directly adjacent to the shock, which is consistent with prior observations, and suggests that they are generated here and damp out as they propagate upstream.

Figure 1 shows that this upstream region also contains higher frequency whistlers ($0.1f_{ce} < f < 0.3f_{ce}$), which have amplitudes near 0.15 nT and propagate parallel to $\vec{B}_0$. Again, similar waves have been previously seen at Earth, both in the free solar wind and electron foreshock, and could indicate the presence of an upstream traveling electron beam that excites a cyclotron resonance (Olson et al., 1969; Y. Zhang et al., 1998).

We focus on the upstream-to-downstream bow shock crossings at 08:22:30 and 08:29:00 (labeled 1 and 3 above Figure 1.b), which occurred 3 - 4 r_v anti-sunward of Venus and together contain a representative sample of whistler waves. Upstream pointing shock normal vectors $\hat{n}$ were found by applying magnetic field coplanarity (Paschmann & Daly, 1998). They suggest shock normal angles $\theta_{\hat{n}-\vec{B}_{0,up}}$ in the ranges of $20°-40°$ and $10°-20°$ for the 08:22:30 and 08:29:00 shocks, respectively. In the same order, the Alfvén Mach numbers of these shocks are about 6 and 8.

Figure 2 shows whistler waves at multiple frequencies during the bow shock crossing at 08:29. The hodograms of the wave in Figure 2, region (a) (hereafter referred to as region 2.a) are bandpass filtered between 20 and 40 Hz. The $\vec{B}$ field hodogram is in the minimum variance plane, and shows coherent circular polarization. The propagation angle relative to the magnetic field $\theta_{\pm\vec{k}-\vec{B}_0}$ here is about 24°.

The orange ellipse in the $\vec{E}$ hodogram is the projection of a circle around $\vec{B}_0$ into the $\vec{E}$ field measurement plane. The size of the circle has been chosen to allow comparison with the data, and is not otherwise motivated. Although the $\vec{E}$ field is not as coherent as the $\vec{B}$ field, it approximately traces out the orange ellipse over two of the three wave cycles plotted, as expected for a quasi-parallel whistler wave.

Their hodograms are not presented, but the waves around 08:29:05.0 are similar, propagating 20° from $\vec{B}_0$ at frequencies near 30 Hz. Both of these example waves are segments of $0.1f_{ce} < f < 0.3f_{ce}$ fluctuation power that grows out of minima in $|B_0|$ and subsequently decays. The events begin with low frequency waves of the type in region 2.b, and higher frequency waves grow as $|B_0|$ increases. A similar pattern is seen from 08:29:05.5 to 08:29:05.8, although the $|B_0|$ trough is substantially shallower here, and the subsequent waves (e.g. in region 2.c) decay more quickly.

Interacting whistler waves at different frequencies have also been observed in Earth's bow shock (Hull et al., 2012, 2020). A band with $f \sim 0.1 - 0.5f_{ce}$ and $\Delta B/|B_0| \sim 0.01$ propagates quasi-parallel to $\vec{B}_0$ and is excited by lower frequency whistlers. The small amplitude waves in regions 2.a and 2.c may be representatives of an analogous band at Venus. At Earth, the low frequency waves are in the range of the lower hybrid frequency (f_{lh}) and propagate oblique to $\vec{B}_0$ with $\Delta B/|B_0| \sim 0.1-1$ (Hull et al., 2020). The relatively large amplitude whistlers in Figure 2 (e.g. in region 2.b, where $\Delta B/|B_0| \sim 0.06$) also propagate oblique to $\vec{B}_0$ and have frequencies similar to the mean of value of f_{lh}, ~5 Hz, in the time span shown.

The region 2.b hodograms are bandpass filtered between 8 and 12 Hz. In $\beta \gtrsim 0.1$ conditions, oblique whistler waves should have elliptical polarization of $\vec{B}$ (Verkhoglyadova et al., 2013; Remya et al., 2016). In region 2.b, $\beta > 1$, so the approximately circular polarization here is surprising. Still, it is clear that $\vec{E}$ and $\vec{B}$ are coupled and constitute an electromagnetic wave – their cross coherence is approximately 1 in a 4 Hz-wide band

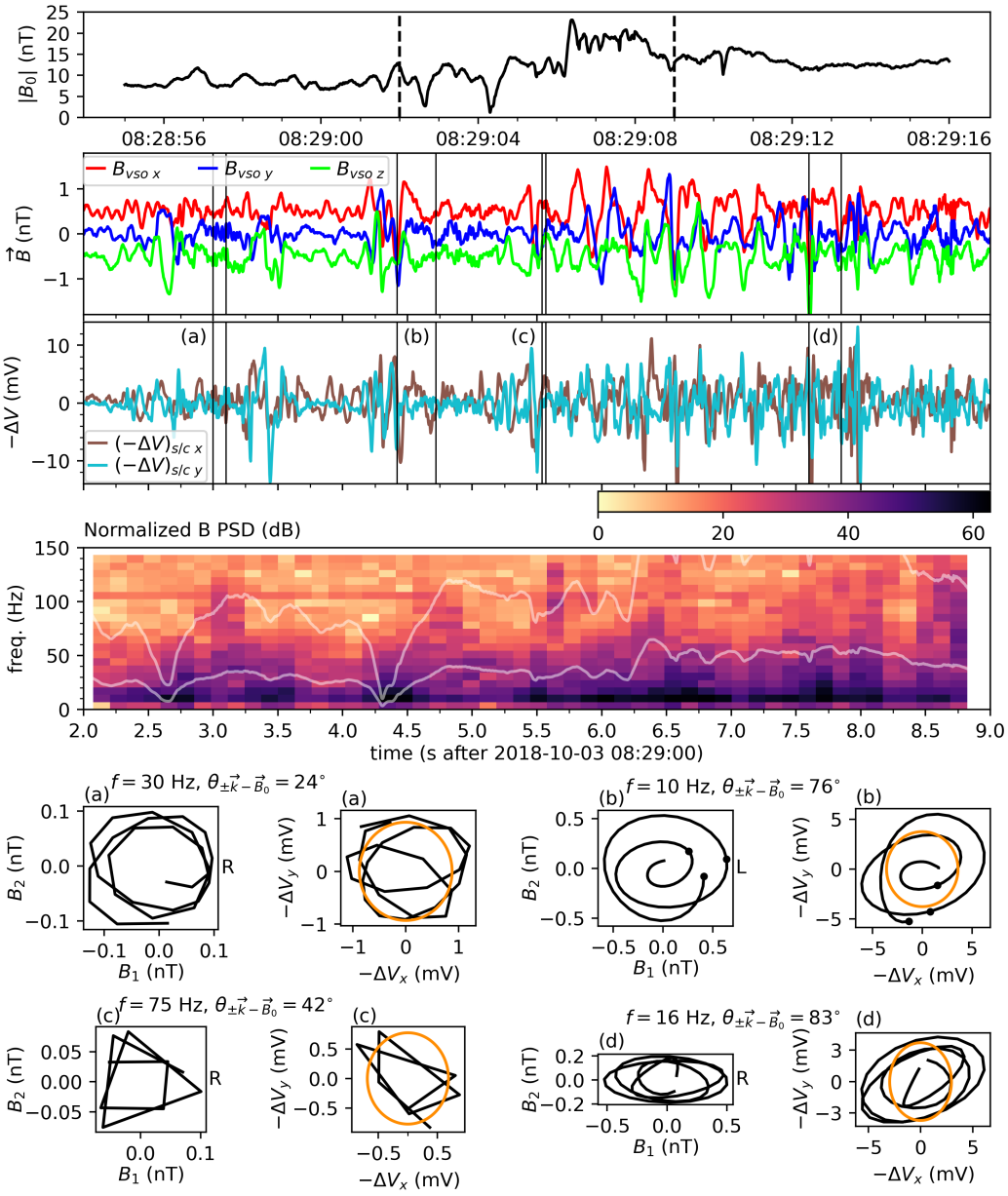

Figure 2. Whistler waves at multiple scales within the bow shock. The top panel shows an overview of the magnetic field magnitude. The vertical dashed black lines mark the time limits of the next three panels. Panels 2 and 3 show magnetic field in VSO coordinates and electric field in spacecraft coordinates; both are high-pass filtered above 4 Hz. We plot the potential differences measured by the antennas instead of the electric field due to lack of knowledge of the effective antenna lengths during this time. For each of the regions labeled (a), (b), (c), and (d), there are two hodograms: one of $\vec{B}$ and one of $\vec{E}$. The $\vec{B}$ field hodogram is in the minimum variance plane. The $\vec{E}$ field hodogram is in the spacecraft X-Y plane. The orange trace is the projection of a circle around $\vec{B}_0$ into the $\vec{E}$ field measurement plane. To the right of each $\vec{B}$ hodogram, either R or L is written, which stand for right- or left-handed rotation of $\vec{B}$ about $\vec{B}_0$. The appearance of left-handed polarization for the region (b) wave is addressed in Section 4.3.

centered at 10 Hz. Black dots have been added to their hodograms at three equally spaced positions starting at $t = 0$. The fields both spiral inwards as the wave decays.

4 $f < 0.1 f_{ce}$ Whistler Waves Propagating $> 80°$ Oblique to $\vec{B}_0$

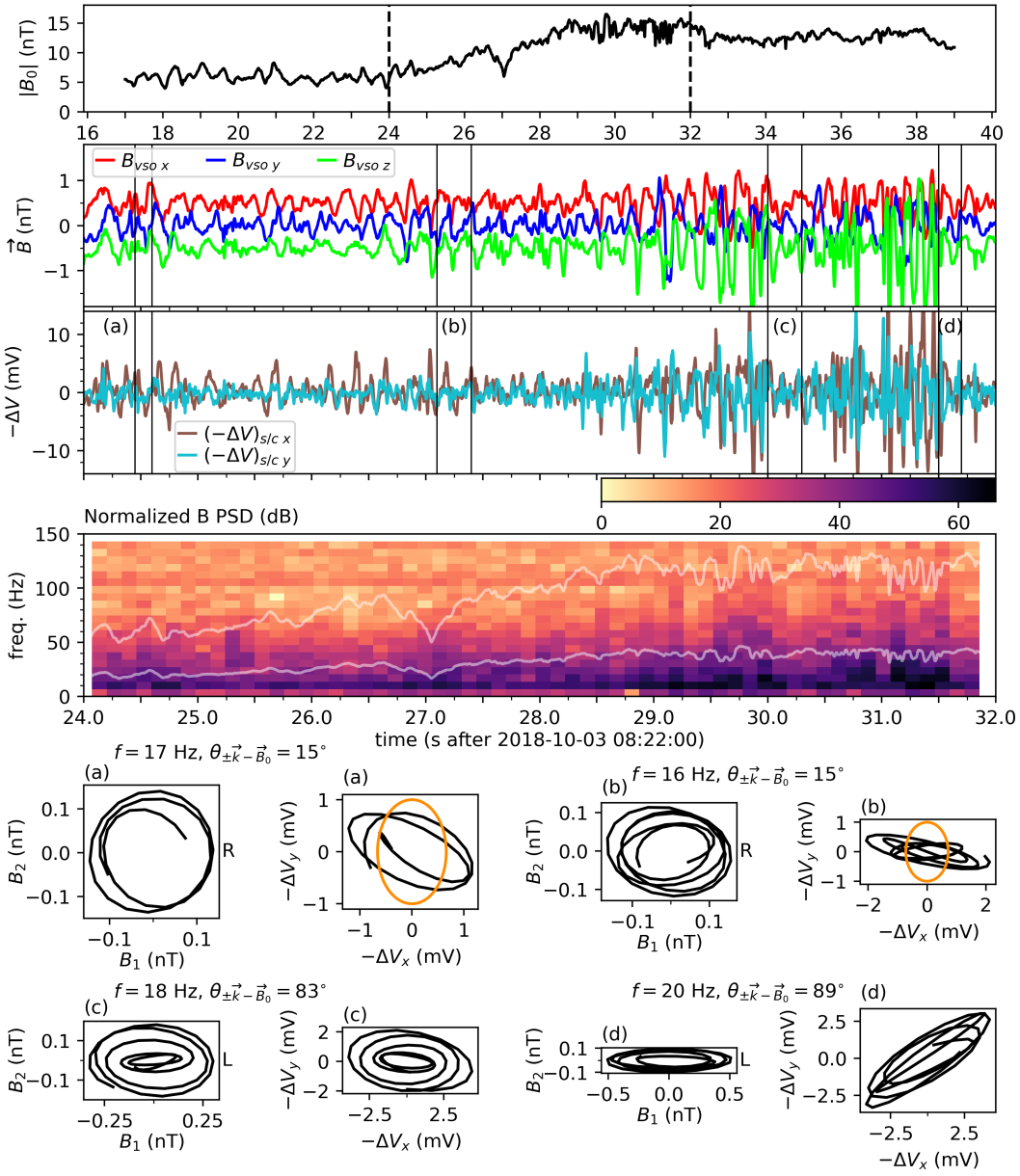

Figure 3. Low frequency whistler waves in the magnetic ramp of the 08:22:30 bow shock crossing. For the quasi-parallel propagating waves in regions (a) and (b), disagreement between the electric field hodograms and the orange ellipse is unexpected, and may be caused by instrumental distortion of the $\vec{E}$ field. The elliptical polarization of $\vec{B}$ seen for the oblique waves in regions (c) and (d) is expected in warm plasmas. These waves have left-handed polarization about $\vec{B}_0$ in the spacecraft frame, which is discussed in Section 4.3 and is likely due to Doppler shifting.

4.1 Polarization of $\vec{B}$

The 08:22:30 bow shock crossing is presented in Figure 3. Downstream of the $\vec{B}_0$ shock discontinuities, the 08:22:30 and 08:29:00 crossings both feature very oblique waves, examples of which are in regions 2.d, 3.c, and 3.d. To isolate these waves from the broadband low frequency spectrum, 2nd order Butterworth filters with 4 Hz-wide passbands were applied to the data. The resulting waveforms have elliptically polarized $\vec{B}$, in agreement with predictions by Verkhoglyadova et al. (2013) for oblique whistlers in warm plasmas. In cold plasmas, $\vec{B}$ is circularly polarized regardless of the propagation angle $\theta_{\vec{k}-\vec{B}_0}$; the observed ellipticity is caused by thermal electron motion (Verkhoglyadova et al., 2010).

We denote the maximum and intermediate variance directions determined by MVA as $\hat{\epsilon}_{MVA\ B,1}$ and $\hat{\epsilon}_{MVA\ B,2}$, respectively. $\hat{z}'$ is defined as the direction (either $\hat{k}$ or -$\hat{k}$) around which $\vec{B}$ rotates in a right-handed sense. Following Verkhoglyadova et al. (2010), we also define $\hat{y}$ as a unit vector in the $\hat{B}_0 \times \hat{z}'$ direction and $\hat{x}' = \hat{y} \times \hat{z}'$.

As illustrated in Figure 4, $\vec{B}$'s semimajor axis should lie in the $\hat{x}'$ direction and its semiminor axis should lie in the $\hat{y}$ direction (Verkhoglyadova et al., 2013; Remya et al., 2016). We find in each of the regions 2.d, 3.c, and 3.d, $|\hat{\epsilon}_{MVA\ B,2} \cdot \hat{y}| > 0.98$, confirming theoretical predictions. $|\hat{\epsilon}_{MVA\ B,1} \cdot \hat{x}'| \sim 1$ naturally follows.

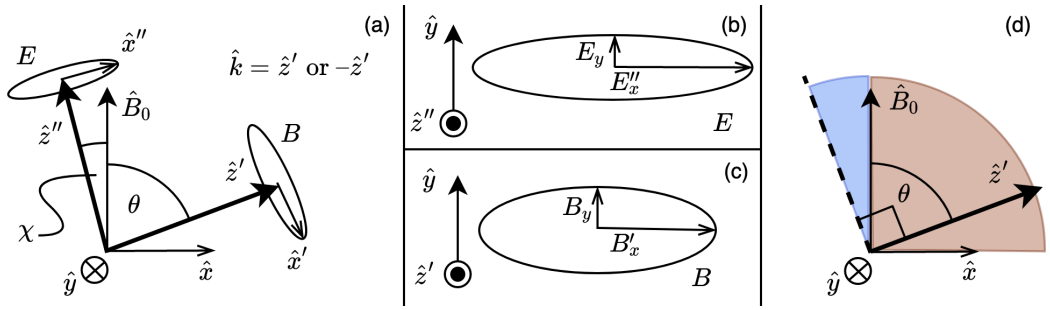

Figure 4. Polarization of oblique whistler waves. Panel (a) demonstrates that $\vec{B}_0$, the polarization axis of $\vec{E}$ ($\hat{z}''$), and the polarization axis of $\vec{B}$ ($\hat{z}'$) are co-planar. Here $\hat{z}'$ and $\hat{z}''$ are defined to be the directions around which $\vec{B}$ and $\vec{E}$ rotate in a right-handed sense. Equation 1 provides a relationship between $\vec{B}$ ellipticity, $\vec{E}$ ellipticity, and $\theta + \chi$. For the wave illustrated, this is satisfied by $|B_y/B'_x| \approx 1/2.75$, $|E''_x/E_y| \approx 4.25$, and $\theta + \chi \approx 85°$. For the direction of $\hat{z}'$ shown, the blue and brown shadings in panel (d) mark allowed orientations for $\hat{z}''$ under various assumptions – the brown sector may not be allowed. See the text for details.

4.2 Polarization of $\vec{E}$

Kinetic theory and Maxwell's equations make predictions for the electric field polarization that we did not observe, most likely due to instrumental effects. For the following, $\hat{z}'$ is again the axis around which $\vec{B}$ rotates in a right-handed sense, and θ is its inclination from $\vec{B}_0$. $\hat{z}''$ is the axis around which $\vec{E}$ rotates in a right-handed sense, and χ is its inclination from $\vec{B}_0$.

For plasma with an electron velocity distribution function of the form $f(v_\perp^2, v_\parallel)$ in a uniform background $\vec{B}_0$, $\hat{z}''$ is coplanar with $\hat{k}$ and $\hat{B}_0$ (Krall & Trivelpiece, 1973; Verkhoglyadova et al., 2013). In addition, from Faraday's law, $\vec{E}$ and $\vec{B}$ must rotate in the same sense about $\hat{k}$, restricting $\hat{z}''$ to lie within 90° of $\hat{z}'$. To produce whistler mode electron dynamics, $\vec{E}$ must also rotate in a right-handed sense about $\hat{B}_0$, likewise restricting $\hat{z}''$ to lie within 90° of $\hat{B}_0$ (Jackson, 1999).

In full, these criteria limit $\hat{z}''$ to a $(180°-\theta)$ span in the $\hat{B}_0-\hat{z}'$ plane. This window is marked by the union of the blue and brown sectors in Figure 4.d. In the cold plasma approximation, Verkhoglyadova et al. (2010) show that $\hat{z}'$ and $\hat{z}''$ are canted to opposite directions with respect to $\vec{B}_0$, so both θ and χ as illustrated in Figure 4.a are positive, and $\hat{z}''$ is limited to the blue sector in Figure 4.d. For the region 2.d, 3.c, and 3.d waves, $\theta_{\pm\vec{k}-\vec{B}_0} > 80°$ with the restrictions $\chi > 0°$ and $\chi + \theta < 90°$ leaves a window for χ smaller than 10°.

Faraday's law also gives information about the ellipticities of $\vec{E}$ and $\vec{B}$ – in the plane perpendicular to $\hat{k}$, they are equal: $|E'_x/E_y| = |B_y/B'_x|$ (Bellan, 2013). This provides a relationship between $\vec{B}$ ellipticity, $\vec{E}$ ellipticity, and the angle of inclination, $\theta+\chi$, between the $\vec{E}$ and $\vec{B}$ polarization planes

$$\frac{E'_x}{E_y} = \frac{E''_x \cos(\theta+\chi)}{E_y} = \frac{B_y}{B'_x} \tag{1}$$

For each position of $\hat{z}''$ in the blue sector in Figure 4.d, Equation 1 was enforced, and the resulting $\vec{E}$ ellipse was projected into the antenna measurement plane and compared with observations. For the waves in regions 2.d, 3.c, and 3.d, this search was unsuccessful.

Allowing for the possibility that the cold plasma stipulation $\chi > 0°$ does not extend to warm plasmas, the same procedure was applied for orientations of $\hat{z}''$ in the brown sector in Figure 4.d, but again agreement with the observed $\vec{E}$ field was not found. This may point to the need for a low frequency correction to the ΔV measured by the antennas. This need is evident in the DC electric field measurements, which often diverge from $-\vec{v}\times\vec{B}$ (Mozer et al., 2020; Bowen et al., 2020).

Regions 3.a and 3.b also indicate that the measured $\vec{E}$ field may be distorted by instrumental effects. These ∼16 Hz waves propagate quasi-parallel to $\vec{B}_0$ and appropriately have circularly polarized $\vec{B}$. The divergences of the $\vec{E}$ field hodograms from the orange ellipses indicate that the measured $\vec{E}$ is not approximately circularly polarized around $\vec{B}_0$, which it should be provided that these waves are whistlers.

4.3 Doppler Shifting and Wave Damping

The region 2.b, 3.c, and 3.d waves have left-handed polarization about $\vec{B}_0$ in the spacecraft frame, so if they are whistlers, a Doppler shift must have inverted their intrinsic right-handed polarization. Alternatively, they could be ion-cyclotron waves (ICW). However, Krauss-Varban et al. (1994) show that the magnetic field of an oblique ICW is predominantly out of the $\vec{k}-\vec{B}_0$ plane, while for the region 3.c and 3.d waves, it is predominantly in this plane. This observed polarization conforms with the whistler branch in both the high frequency (Verkhoglyadova et al., 2013; Remya et al., 2016) and low frequency fast/magnetosonic regimes (Krauss-Varban et al., 1994).

Provided that the waves are whistlers, their plasma frame frequencies must lie below the resonance frequency $f_{ce}\cos(\theta_{\pm\vec{k}-\vec{B}_0})$, which is in the tens of Hz range. The observed 20 Hz left-handed rotation would then require a Doppler shift $\Delta f = |\hat{k}\cdot\vec{v}_{plasma}|/\lambda$ in the range of 20–100 Hz. Here $\vec{v}_{plasma}$ is the velocity of the plasma in the spacecraft frame, λ is the wavelength, and $\hat{k}\cdot\vec{v}_{plasma}$ must be negative to shift from right-handed to left-handed polarization. For these waves, $|\hat{k}\cdot\vec{v}| \sim 200$ km/s, giving wavelengths $\lambda \sim 2-10$ km. This is similar to the electron inertial length in this region: $k_\perp c/\omega_{pe} \sim 0.6-3$, where $k_\perp$ is the perpendicular wavenumber $(2\pi/\lambda)\sin(\theta_{\pm\vec{k}-\vec{B}_0})$ and ω_{pe} is the electron plasma frequency $\sqrt{n_e e^2/(m_e\epsilon_0)}$. In this regime, the waves undergo electron Landau damping, but at a rate that allows them to persist for several cycles (e.g. Gary & Smith, 2009).

The polarization of $\vec{B}$ in the region 2.b wave is not unique to whistler waves or ion-cyclotron waves, so cannot be used to distinguish between modes. However, a different method can be used to rule out the ICW. The wave's spacecraft frame frequency, f_{sc} =10 Hz, is much larger than the ion-cyclotron frequency, so if the wave is an ICW, f_{sc} is almost entirely due to Doppler shifting: $f_{sc} \approx \hat{k} \cdot \vec{v}_{plasma}/\lambda$. This gives a wavelength of about 20 km, which is much smaller than the ion inertial length: $k_\perp c/\omega_{pi} \sim 13$. Gary and Smith (2009) show that this results in a damping rate that is much faster than the wave frequency, preventing propagation.

5 Conclusions

Whistlers are a prominent feature of the low frequency dynamics in the Venusian bow shock. In the shock transition region, waves with $f \lesssim 0.1 f_{ce}$ preferentially grow out of minima in $|B_0|$, and can be oblique (2.b) or parallel-propagating (3.b). Higher frequency waves with $0.1 f_{ce} < f < 0.4 f_{ce}$ (2.a, 2.c) are strongest in the downstream ramps of these $|B_0|$ minima.

Bandpass filtering the erratic electric and magnetic fields downstream of the shock discontinuity in $\vec{B}_0$ reveals oblique, elliptically polarized whistlers (2.d, 3.c, 3.d). The orientations of the semiminor and semimajor axes of these waves' $\vec{B}$ field ellipses are found to agree with predictions from kinetic theory to high accuracy. This demonstrates that thermal electron motion can have a pronounced effect on whistler wave polarization in plasmas accessible to spacecraft.

The same waves may also be present downstream of Earth's bow shock. Here, MMS measures 3D electric and magnetic fields, so the polarization properties of these waves could be examined in more detail (Burch et al., 2016). If sufficiently well understood, the waves could serve as a window into thermal electron motion in the turbulent plasma downstream of magnetized collisionless shocks.

Acknowledgments

The FIELDS and SWEAP instruments on the Parker Solar Probe spacecraft were designed and developed under NASA contract NNN06AA01C. Data from these instruments are publicly available:

FIELDS: https://fields.ssl.berkeley.edu/data/

SWEAP: http://sweap.cfa.harvard.edu/Data.html

References

Bale, S. D., Goetz, K., Harvey, P. R., Turin, P., Bonnell, J. W., Dudok de Wit, T., ... Wygant, J. R. (2016, Dec 01). The fields instrument suite for solar probe plus. *Space Science Reviews*, *204*(1), 49-82. Retrieved from `https://doi.org/10.1007/s11214-016-0244-5` doi: 10.1007/s11214-016-0244-5

Bellan, P. M. (2013). Circular polarization of obliquely propagating whistler wave magnetic field. *Physics of Plasmas*, *20*(8), 082113. Retrieved from `https://doi.org/10.1063/1.4817964` doi: 10.1063/1.4817964

Bowen, T. A., Bale, S. D., Bonnell, J., Larson, D., Mallet, A., McManus, M. D., ... Psp/Sweap Teams (2020, Aug). The Electromagnetic Signature of Outward Propagating Ion-scale Waves. *The Astrophysical Journal*, *899*(1), 74. doi: 10.3847/1538-4357/ab9f37

Bowen, T. A., Bale, S. D., Bonnell, J. W., Dudok de Wit, T., Goetz, K., Goodrich, K., ... Szabo, A. (2020). A merged search-coil and fluxgate magnetometer data product for parker solar probe fields. *Journal of Geophysical Research: Space Physics*, *125*(5), e2020JA027813. Retrieved from `https://agupubs.onlinelibrary.wiley.com/doi/abs/10.1029/2020JA027813` (e2020JA027813 10.1029/2020JA027813) doi: 10.1029/2020JA027813

Brain, D. A., Bagenal, F., AcuÃa, M. H., Connerney, J. E. P., Crider, D. H., Mazelle, C., ... Ness, N. F. (2002). Observations of low-frequency electromagnetic plasma waves upstream from the martian shock. *Journal of Geophysical Research: Space Physics*, *107*(A6), SMP 9-1-SMP 9-11. Retrieved from `https://agupubs.onlinelibrary.wiley.com/doi/abs/10.1029/2000JA000416` doi: 10.1029/2000JA000416

Burch, J. L., Moore, T. E., Torbert, R. B., & Giles, B. L. (2016). Magnetospheric multiscale overview and science objectives. *Space Science Reviews*, *199*(1-4), 5-21. doi: 10.1007/s11214-015-0164-9

Case, A. W., Kasper, J. C., Stevens, M. L., Korreck, K. E., Paulson, K., Daigneau, P., ... Martinović, M. M. (2020, feb). The solar probe cup on the parker solar probe. *The Astrophysical Journal Supplement Series*, *246*(2), 43. Retrieved from `https://doi.org/10.3847%2F1538-4365%2Fab5a7b` doi: 10.3847/1538-4365/ab5a7b

Fairfield, D. H. (1974). Whistler waves observed upstream from collisionless shocks. *Journal of Geophysical Research (1896-1977)*, *79*(10), 1368-1378. Retrieved from `https://agupubs.onlinelibrary.wiley.com/doi/abs/10.1029/JA079i010p01368` doi: 10.1029/JA079i010p01368

Gary, S. P., & Smith, C. W. (2009). Short-wavelength turbulence in the solar wind: Linear theory of whistler and kinetic alfvÃ©n fluctuations. *Journal of Geophysical Research: Space Physics*, *114*(A12). Retrieved from `https://agupubs.onlinelibrary.wiley.com/doi/abs/10.1029/2009JA014525` doi: 10.1029/2009JA014525

Holzer, R. E., Northrop, T. G., Olson, J. V., & Russell, C. T. (1972). Study of waves in the earth's bow shock. *Journal of Geophysical Research (1896-1977)*, *77*(13), 2264-2273. Retrieved from `https://agupubs.onlinelibrary.wiley.com/doi/abs/10.1029/JA077i013p02264` doi: 10.1029/JA077i013p02264

Hull, A. J., Muschietti, L., Le Contel, O., Dorelli, J. C., & Lindqvist, P.-A. (2020).

Mms observations of intense whistler waves within earth's supercritical bow shock: Source mechanism and impact on shock structure and plasma transport. *Journal of Geophysical Research: Space Physics*, *125*(7), e2019JA027290. Retrieved from https://agupubs.onlinelibrary.wiley.com/doi/abs/10.1029/2019JA027290 (e2019JA027290 10.1029/2019JA027290) doi: 10.1029/2019JA027290

Hull, A. J., Muschietti, L., Oka, M., Larson, D. E., Mozer, F. S., Chaston, C. C., ... Hospodarsky, G. B. (2012). Multiscale whistler waves within earth's perpendicular bow shock. *Journal of Geophysical Research: Space Physics*, *117*(A12). Retrieved from https://agupubs.onlinelibrary.wiley.com/doi/abs/10.1029/2012JA017870 doi: 10.1029/2012JA017870

Jackson, J. D. (1999). Classical electrodynamics. In (3rd ed. ed., p. 316-317). New York, NY: Wiley.

Kasper, J. C., Abiad, R., Austin, G., Balat-Pichelin, M., Bale, S. D., Belcher, J. W., ... others (2016). Solar wind electrons alphas and protons (sweap) investigation: design of the solar wind and coronal plasma instrument suite for solar probe plus. *Space Science Reviews*, *204*(1-4), 131–186.

Krall, N. A., & Trivelpiece, A. W. (1973). Principles of plasma physics. krall. In (p. 402-407). New York: McGraw-Hill.

Krauss-Varban, D., Omidi, N., & Quest, K. B. (1994). Mode properties of low-frequency waves: Kinetic theory versus hall-mhd. *Journal of Geophysical Research: Space Physics*, *99*(A4), 5987-6009. Retrieved from https://agupubs.onlinelibrary.wiley.com/doi/abs/10.1029/93JA03202 doi: 10.1029/93JA03202

Malaspina, D. M., Ergun, R. E., Bolton, M., Kien, M., Summers, D., Stevens, K., ... Goetz, K. (2016). The digital fields board for the fields instrument suite on the solar probe plus mission: Analog and digital signal processing. *Journal of Geophysical Research: Space Physics*, *121*(6), 5088-5096. Retrieved from https://agupubs.onlinelibrary.wiley.com/doi/abs/10.1002/2016JA022344 doi: 10.1002/2016JA022344

Mozer, F. S., Agapitov, O. V., Bale, S. D., Bonnell, J. W., Bowen, T. A., & Vasko, I. (2020). Dc and low-frequency electric field measurements on the parker solar probe. *Journal of Geophysical Research: Space Physics*, *125*(9), e2020JA027980. Retrieved from https://agupubs.onlinelibrary.wiley.com/doi/abs/10.1029/2020JA027980 (e2020JA027980 2020JA027980) doi: 10.1029/2020JA027980

Oka, M., III, L. B. W., Phan, T. D., Hull, A. J., Amano, T., Hoshino, M., ... Lindqvist, P. A. (2017, jun). Electron scattering by high-frequency whistler waves at earth's bow shock. *The Astrophysical Journal*, *842*(2), L11. Retrieved from https://doi.org/10.3847%2F2041-8213%2Faa7759 doi: 10.3847/2041-8213/aa7759

Oka, M., Otsuka, F., Matsukiyo, S., Wilson, L. B., Argall, M. R., Amano, T., ... Lindqvist, P. A. (2019, nov). Electron scattering by low-frequency whistler waves at earth's bow shock. *The Astrophysical Journal*, *886*(1), 53. Retrieved from https://doi.org/10.3847%2F1538-4357%2Fab4a81 doi: 10.3847/1538-4357/ab4a81

Olson, J. V., Holzer, R. E., & Smith, E. J. (1969). High-frequency magnetic fluctuations associated with the earth's bow shock. *Journal of Geophysical Research (1896-1977)*, *74*(19), 4601-4617. Retrieved from https://agupubs.onlinelibrary.wiley.com/doi/abs/10.1029/JA074i019p04601 doi: 10.1029/JA074i019p04601

Orlowski, D. S., & Russell, C. T. (1991). Ulf waves upstream of the venus bow shock: Properties of one-hertz waves. *Journal of Geophysical Research: Space Physics*, *96*(A7), 11271-11282. Retrieved from https://agupubs.onlinelibrary.wiley.com/doi/abs/10.1029/91JA01103 doi:

10.1029/91JA01103

Paschmann, G., & Daly, P. W. (1998, January). Analysis Methods for Multi-Spacecraft Data. ISSI Scientific Reports Series SR-001, ESA/ISSI, Vol. 1. ISBN 1608-280X, 1998. *ISSI Scientific Reports Series*, *1*.

Remya, B., Lee, K. H., Lee, L. C., & Tsurutani, B. T. (2016). Polarization of obliquely propagating whistler mode waves based on linear dispersion theory. *Physics of Plasmas*, *23*(12), 122120. Retrieved from https://doi.org/10.1063/1.4972534 doi: 10.1063/1.4972534

Rodriguez, P., & Gurnett, D. A. (1975). Electrostatic and electromagnetic turbulence associated with the earth's bow shock. *Journal of Geophysical Research (1896-1977)*, *80*(1), 19-31. Retrieved from https://agupubs.onlinelibrary.wiley.com/doi/abs/10.1029/JA080i001p00019 doi: 10.1029/JA080i001p00019

Scarf, F. L., Taylor, W. W. L., Russell, C. T., & Elphic, R. C. (1980). Pioneer venus plasma wave observations: The solar wind-venus interaction. *Journal of Geophysical Research: Space Physics*, *85*(A13), 7599-7612. Retrieved from https://agupubs.onlinelibrary.wiley.com/doi/abs/10.1029/JA085iA13p07599 doi: 10.1029/JA085iA13p07599

Sonnerup, B. U., & Scheible, M. (1998). Minimum and maximum variance analysis. *Analysis methods for multi-spacecraft data*, 185–220.

Strangeway, R. J., & Crawford, G. K. (1993). On the instability and energy flux of lower hybrid waves in the venus plasma mantle. *Geophysical Research Letters*, *20*(12), 1211-1214. Retrieved from https://agupubs.onlinelibrary.wiley.com/doi/abs/10.1029/93GL01354 doi: 10.1029/93GL01354

Szegö, K., Shapiro, V. S., Shevchenko, V. I., Sagdeev, R. Z., Kasprzak, W. T., & Nagy, A. F. (1991). Physical processes in the plasma mantle of venus. *Geophysical Research Letters*, *18*(12), 2305-2308. Retrieved from https://agupubs.onlinelibrary.wiley.com/doi/abs/10.1029/91GL02086 doi: 10.1029/91GL02086

Verkhoglyadova, O. P., Tsurutani, B. T., & Lakhina, G. S. (2010). Properties of obliquely propagating chorus. *Journal of Geophysical Research: Space Physics*, *115*(A9). Retrieved from https://agupubs.onlinelibrary.wiley.com/doi/abs/10.1029/2009JA014809 doi: 10.1029/2009JA014809

Verkhoglyadova, O. P., Tsurutani, B. T., & Lakhina, G. S. (2013). Theoretical analysis of poynting flux and polarization for elf-vlf electromagnetic waves in the earth's magnetosphere. *Journal of Geophysical Research: Space Physics*, *118*(12), 7695-7702. Retrieved from https://agupubs.onlinelibrary.wiley.com/doi/abs/10.1002/2013JA019371 doi: 10.1002/2013JA019371

Whittlesey, P. L., Larson, D. E., Kasper, J. C., Halekas, J., Abatcha, M., Abiad, R., ... Verniero, J. L. (2020, mar). The solar probe ANalyzers—electrons on the parker solar probe. *The Astrophysical Journal Supplement Series*, *246*(2), 74. Retrieved from https://doi.org/10.3847%2F1538-4365%2Fab7370 doi: 10.3847/1538-4365/ab7370

Wilson III, L. B., Sibeck, D. G., Breneman, A. W., Contel, O. L., Cully, C., Turner, D. L., ... Malaspina, D. M. (2014). Quantified energy dissipation rates in the terrestrial bow shock: 2. waves and dissipation. *Journal of Geophysical Research: Space Physics*, *119*(8), 6475-6495. Retrieved from https://agupubs.onlinelibrary.wiley.com/doi/abs/10.1002/2014JA019930 doi: 10.1002/2014JA019930

Xiao, S., Wu, M., Wang, G., Chen, Y., & Zhang, T. (2020). Survey of 1-hz waves in the near-venusian space: Venus express observations. *Planetary and Space Science*, *187*, 104933. Retrieved from http://www.sciencedirect.com/science/article/pii/S0032063320300532 doi: https://doi.org/10.1016/j.pss.2020.104933

Zhang, T., Delva, M., Baumjohann, W., Volwerk, M., Russell, C., Barabash, S., ...

Zambelli, W. (2008). Initial venus express magnetic field observations of the venus bow shock location at solar minimum. *Planetary and Space Science*, *56*(6), 785 - 789. Retrieved from http://www.sciencedirect.com/science/article/pii/S0032063307003777 (Mars Express/Venus Express) doi: https://doi.org/10.1016/j.pss.2007.09.012

Zhang, Y., Matsumoto, H., & Kojima, H. (1998). Bursts of whistler mode waves in the upstream of the bow shock: Geotail observations. *Journal of Geophysical Research: Space Physics*, *103*(A9), 20529-20540. Retrieved from https://agupubs.onlinelibrary.wiley.com/doi/abs/10.1029/98JA01371 doi: 10.1029/98JA01371

Zhang, Y., Matsumoto, H., Kojima, H., & Omura, Y. (1999). Extremely intense whistler mode waves near the bow shock: Geotail observations. *Journal of Geophysical Research: Space Physics*, *104*(A1), 449-461. Retrieved from https://agupubs.onlinelibrary.wiley.com/doi/abs/10.1029/1998JA900049 doi: 10.1029/1998JA900049

new_bs2_rev2.png.

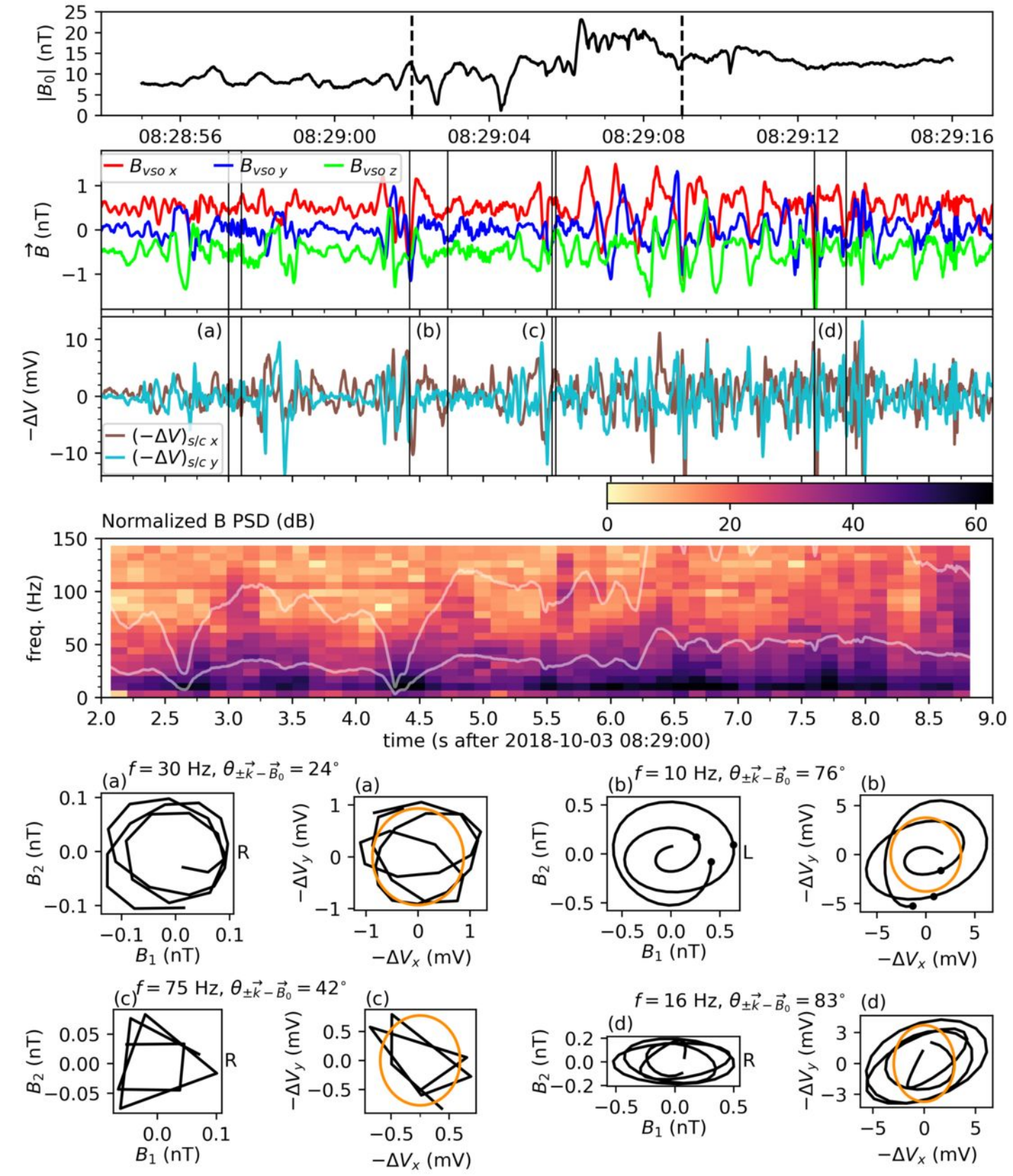
$|B_0|$ (nT)
08:28:56
08:29:00
08:29:04
08:29:08
08:29:12
08:29:16
$B_{vso\ x}$
$B_{vso\ y}$
$B_{vso\ z}$
$\vec{B}$ (nT)
(a)
(b)
(c)
(d)
$-\Delta V$ (mV)
$(-\Delta V)_{s/c\ x}$
$(-\Delta V)_{s/c\ y}$
Normalized B PSD (dB)
freq. (Hz)
time (s after 2018-10-03 08:29:00)
$f = 30$ Hz, $\theta_{\pm\vec{k}-\vec{B}_0} = 24°$
$f = 10$ Hz, $\theta_{\pm\vec{k}-\vec{B}_0} = 76°$
$f = 75$ Hz, $\theta_{\pm\vec{k}-\vec{B}_0} = 42°$
$f = 16$ Hz, $\theta_{\pm\vec{k}-\vec{B}_0} = 83°$
B_2 (nT)
B_1 (nT)
$-\Delta V_y$ (mV)
$-\Delta V_x$ (mV)
R
L

new_new_overview.png.

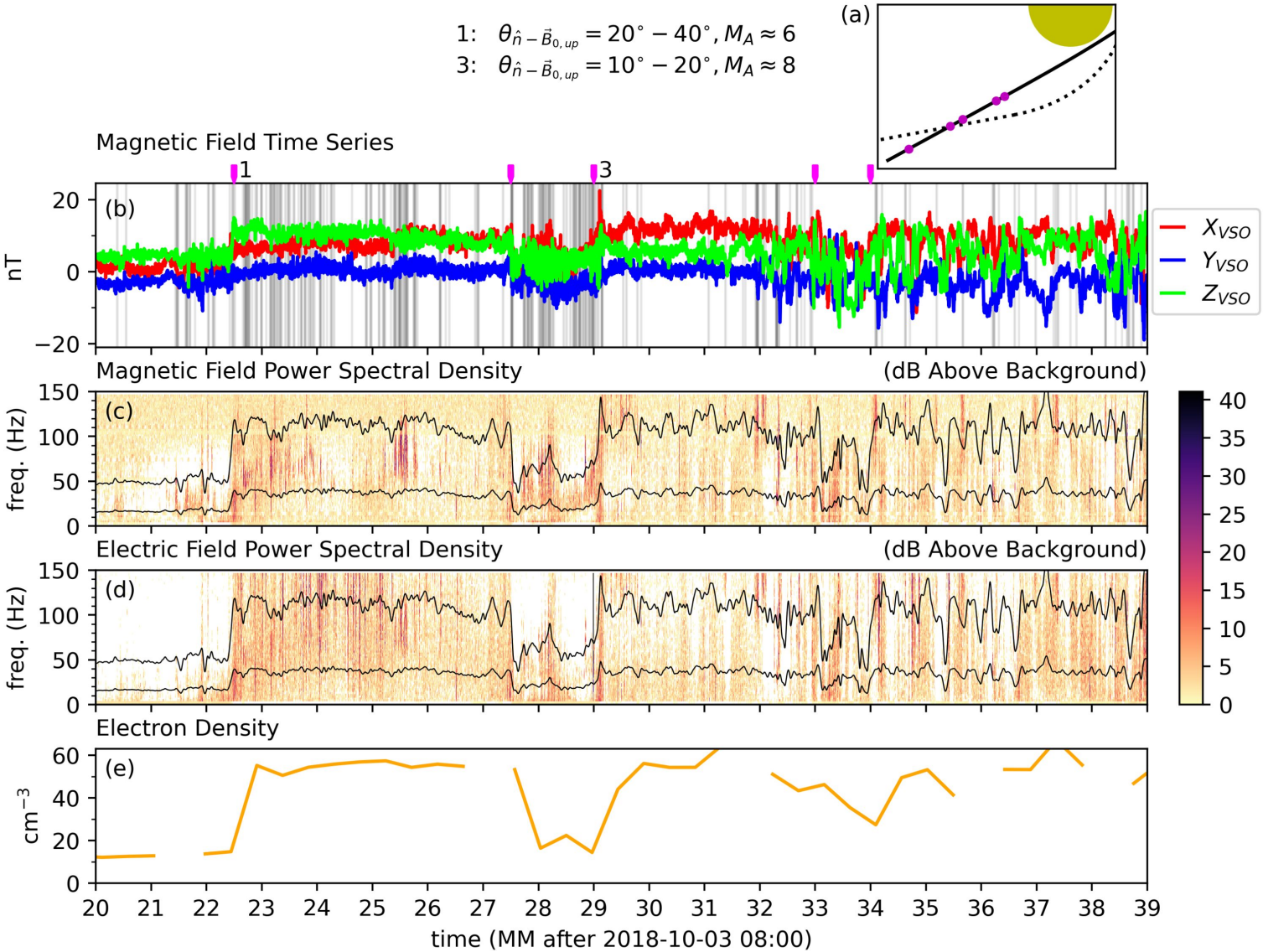
1: $\theta_{\hat{n}-\vec{B}_{0,up}} = 20^\circ - 40^\circ, M_A \approx 6$
3: $\theta_{\hat{n}-\vec{B}_{0,up}} = 10^\circ - 20^\circ, M_A \approx 8$
(a)
Magnetic Field Time Series
1
3
(b)
nT
20
0
−20
X_{VSO}
Y_{VSO}
Z_{VSO}
Magnetic Field Power Spectral Density
(dB Above Background)
(c)
freq. (Hz)
150
100
50
0
40
35
30
25
20
15
10
5
0
Electric Field Power Spectral Density
(dB Above Background)
(d)
freq. (Hz)
Electron Density
(e)
cm^{-3}
60
40
20
0
20
21
22
23
24
25
26
27
28
29
30
31
32
33
34
35
36
37
38
39
time (MM after 2018-10-03 08:00)

new_bs1_rev2.png.

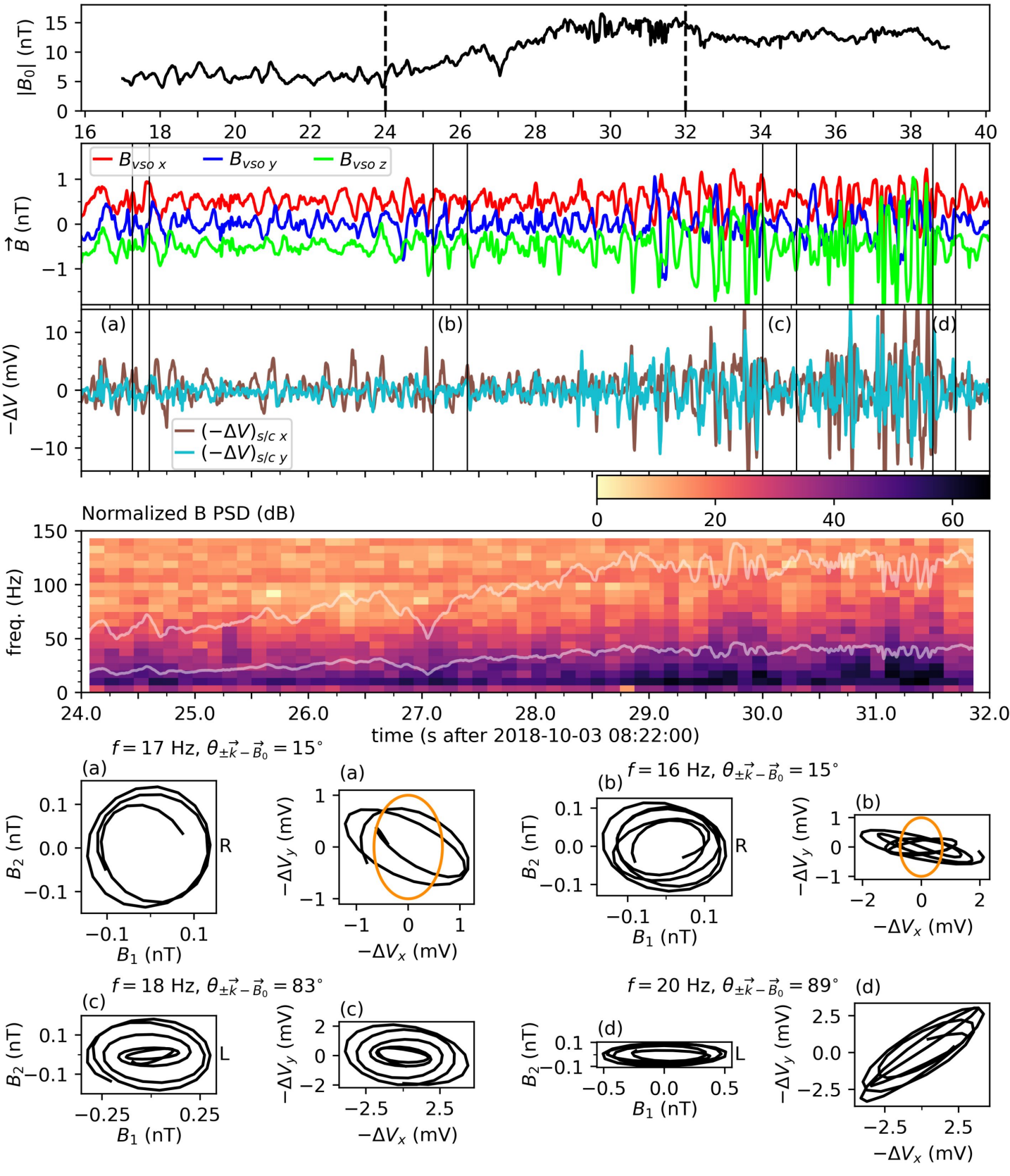
$|B_0|$ (nT)
$B_{vso\ x}$
$B_{vso\ y}$
$B_{vso\ z}$
$\vec{B}$ (nT)
(a)
(b)
(c)
(d)
$-\Delta V$ (mV)
$(-\Delta V)_{s/c\ x}$
$(-\Delta V)_{s/c\ y}$
Normalized B PSD (dB)
freq. (Hz)
time (s after 2018-10-03 08:22:00)
$f = 17$ Hz, $\theta_{\pm\vec{k}-\vec{B}_0} = 15°$
$f = 16$ Hz, $\theta_{\pm\vec{k}-\vec{B}_0} = 15°$
$f = 18$ Hz, $\theta_{\pm\vec{k}-\vec{B}_0} = 83°$
$f = 20$ Hz, $\theta_{\pm\vec{k}-\vec{B}_0} = 89°$
B_2 (nT)
B_1 (nT)
$-\Delta V_y$ (mV)
$-\Delta V_x$ (mV)
R
L

new_ob_ww_diag.png.

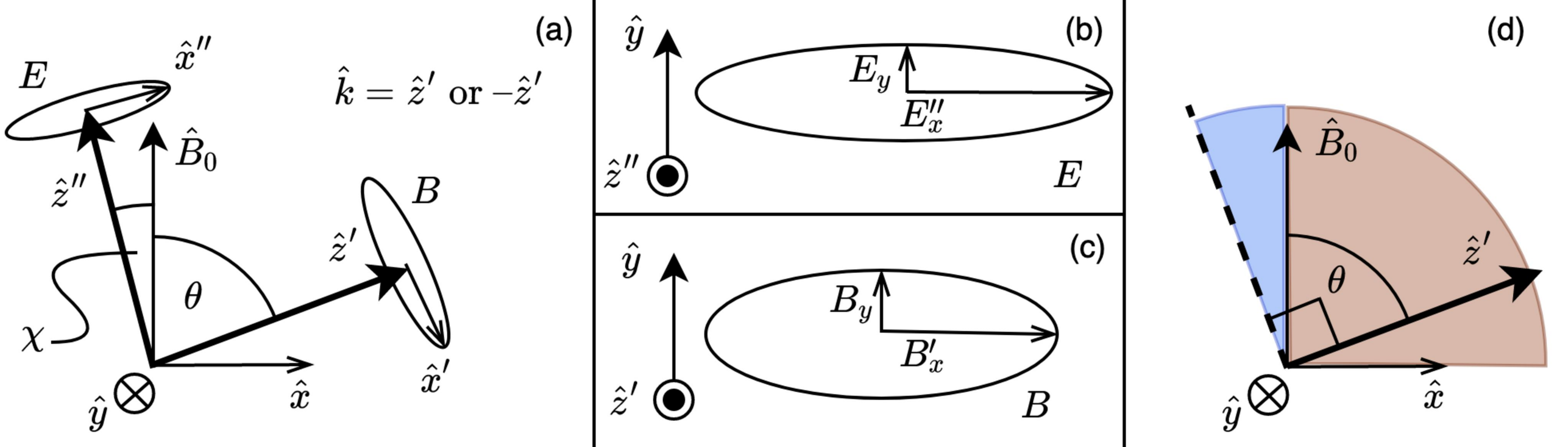
(a)
E
$\hat{x}''$
$\hat{k} = \hat{z}'$ or $-\hat{z}'$
$\hat{B}_0$
$\hat{z}''$
B
$\hat{z}'$
θ
χ
$\hat{y}$
$\hat{x}$
$\hat{x}'$
(b)
$\hat{y}$
E_y
E''_x
$\hat{z}''$
E
(c)
$\hat{y}$
B_y
B'_x
$\hat{z}'$
B
(d)
$\hat{B}_0$
$\hat{z}'$
θ
$\hat{y}$
$\hat{x}$